Journal of Imaging Science and Technology® 54(3): 030401–030401-6, 2010.

Multispectral Colormapping Using Penalized Least Square Regression

Bjørn S. Dissing, Jens M. Carstensen and Rasmus Larsen
Department of Informatics and Mathematical Modeling, Technical University of Denmark, Lyngby, Denmark
E-mail: bdi@imm.dtu.dk

Abstract. *The authors propose a novel method to map a multispectral image into the device independent color space CIE-XYZ. This method provides a way to visualize multispectral images by predicting colorvalues from spectral values while maintaining interpretability and is tested on a light emitting diode based multispectral system with a total of 11 channels in the visible area. To obtain interpretable models, the method estimates the projection coefficients with regard to their neighbors as well as the target. This results in relatively smooth coefficient curves which are correlated with the CIE-XYZ color matching functions. The target of the regression is a well known color chart, and the models are validated using leave one out cross validation in order to maintain best possible generalization ability. The authors compare the method with a direct linear regression and see that the interpretability improves significantly but comes at the cost of slightly worse predictability. © 2010 Society for Imaging Science and Technology.*
[DOI: 10.2352/J.ImagingSci.Technol.2010.54.3.030401]

INTRODUCTION

The majority of today's color images are acquired with a charge coupled device (CCD) or complementary metal-oxide semiconductor chip equipped with a Bayer filter i.e., a mosaic filter which splits the incoming photons into three broad primary channels representing the colors or variables; red, green, and blue (RGB). Exactly three variables were according to Grassman[1,2] enough to describe a color sensation.

The usual camera model, assuming Lambertian surfaces, is modeled as a linear transformation [Eq. (1)],

$$P_i = \int_{\lambda} Q_i(\lambda) R_i(\lambda) E_i(\lambda) d\lambda + \epsilon, \tag{1}$$

integrating the light source spectrum E, the surface reflection R, and the sensor spectral sensibility Q over the visible region of the electromagnetic spectrum for the ith camera channel, $i=1, 2, 3$ for standard color images. ϵ is the molling error, assumed Gaussian.

This way of capturing color has definitely proven itself usable, but unfortunately it also has some drawbacks. The rough splitting of the photons has the consequence that the intensity recorded in each channel is an integration over a large range of wavelengths. This means that the spectral radiant power distribution of the scene remains hidden for the camera and can lead to metameric failure. Metameric failure can shortly be explained as when two objects match colorimetrically under one illumination but differ under another. This is because the spectral radiant power distribution of the two objects are different, but the rough splitting of photons fail to observe this. Another drawback of the traditional RGB image acquisition technique is that the colors recorded are device dependent. This means that all cameras records the same scene slightly different, in their own color space.

One way to overcome the problems with metameric failure as well as device dependent colors is by using multispectral imaging systems. In a multispectral image system, the electromagnetic spectrum is sampled more often and in more narrow banded intervals than the three broad intervals used in standard RGB imaging. This means that an approximation of the true distribution of incoming photons is known for each pixel in the image.

There are different ways of creating multispectral images. One approach is to use a set of narrow-band filters which basically makes a more delicate grouping of the reflected light from the scene. A setup used often, e.g., Ref. 3 and more recently in Ref. 4, is the filter wheel approach, where a turnable wheel with different filters is mounted between the lens and the CCD chip. Instead of using a filter wheel, another solution is the crystal liquid tunable filter.[5,6] Videometer[7] has commercialized a multispectral imaging system based on a light emitting diode (LED) technology. Here, a set of LEDs are strobing successively, and an image is recorded for each LED. Further description of this camera can be found in next section.

In the well established ICC color profile system, color is transferred between different devices by use of a profile connection space (PCS) which is an independent color space, either CIE-XYZ or CIE-LAB. The mapping from a device dependent color space to PCS is well investigated and described in, e.g., Refs. 3 and 8–11 where the most common methods used are direct linear regression or regression using polynomials of various degree. Similarly, when using a multispectral device, such as a multispectral imaging system, there is a need to be able to map the multispectral images into PCS. Such a mapping routine is not a trivial task and is the motivation for this article. In Ref. 12 the authors introduce the spectral image processing system (SIPS), where a

Received Sep. 16, 2009; accepted for publication Mar. 18, 2010; published online May 3, 2010.
1062-3701/2010/54(3)/030401/6/$20.00.

visualization is based on spectral angle mapping (SAM) and[13] creates an extension to the SAM based visualization algorithm. Furthermore[13] gives a thorough investigation and description of the requirements for successful mapping from a multispectral space to a three dimensional color space in a set of nine visualization goals. As an alternative to multispectral images, which may have problems with acquisition speed and proper calibration, spectral reconstruction methods offer a way to estimate the reflection spectrum of the sample object. Many different methods have been proposed to create this reconstruction, some of them being.[14–19] As a well established method in this area is the Wiener method[19] which makes use of *a priori* knowledge to build a reconstruction matrix which is multiplied onto the camera response to reconstruct the reflection spectra. Normally spectral reconstruction techniques are used together with normal RGB cameras, but certainly the precision increases with the amount of bands recorded.

In general there are two approaches to transform native camera response to device independent color space. These approaches are using an analytical method as described above or by first estimating the spectral functions as also described above and then convert it to an independent color space. This article uses an analytical method by transforming a multispectral image to the independent color space CIE-XYZ using a regression model, as done in previous studies including Refs. 3 and 20–22. Here, direct regression or regression of a polynomial basis expansion of the camera response was used for the mapping. As alternative to these previous studies we here make use of a regression technique which penalizes the curvature of the regression coefficients instead of direct regression. The idea of this penalization, inspired by Refs. 23 and 24, is to be able to get more smooth, less noisy, and more interpretable models.

A set of training data is needed in order to calibrate the model properly. Different standards could be used for this, such as the NCS color system which covers a vast amount of colors. We have made use of a well known color rendition chart, *X-rite color checker standard*,[25,26] containing 24 squares of different spectral simulations of various common colors as, e.g., light and dark human skins.

IMAGE ACQUISITION AND DATA

The acquisition of data is done using VideometerLab which acquires multi spectral images in up to 20 different wavelengths ranging from 385 to 970 nm. VideometerLab is a multipurpose camera often used for scientific purpose and proof of concept applications, which is why diodes emitting light outside as well as inside the visible area of the electro magnetic spectrum is mounted. Previously this device has been used in many different vision applications. A few examples are quality estimation of mink fur, analysis of psoriasis lesions, classification of fungi, and temporal change detection in reflectance of vegetables.[27–29]

The camera setup is seen in Figure 1(a). The object is placed inside an integrating Ulbricht sphere which has its interior coated with a matte coating to obtain high diffuse

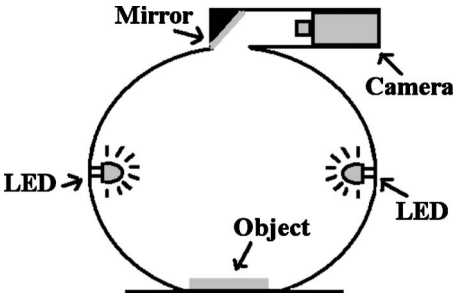

(a)

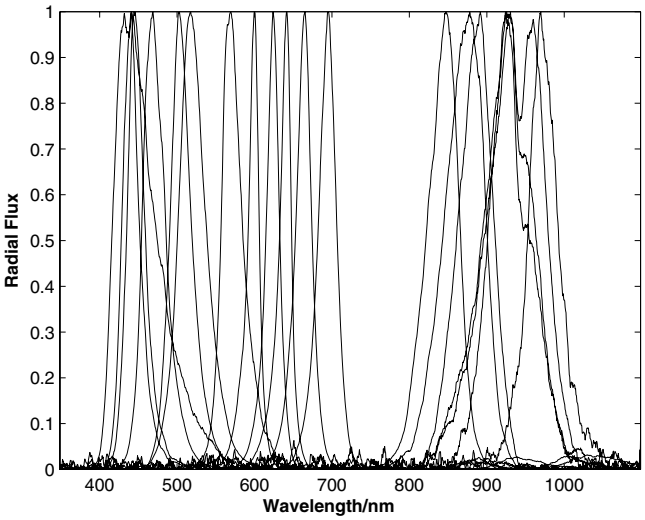

(b)

Figure 1. (a) Principle of imaging with integrating (Ulbricht) sphere illumination. The LEDs located in the rim of the sphere ensures narrowband illumination. (b) Normalized spectral power distributions of the LEDs located in the VideometerLab. (c) Spectral sensitivity of the camera mounted in VideometerLab. It is seen in (a) that the camera is placed above the object of interest.

reflectivity for optimal light conditions. By optimal light conditions is meant conditions which avoid shadows to a certain degree as well as highlights/reflections. In the top of the sphere a Point Gray Scorpion camera is mounted. The LEDs having the spectral radiant power distributions seen in Fig. 1(b) are strobing successively, and for each LED an image of dimensionality 1280×960 is acquired, which in the end yields a multispectral image. In general, not many multispectral imaging systems using LEDs exists, however[30] introduces a camera system which employs a LED array coupled with a photodiode array to measure reflectance spectra. Their system is evaluated by its ability to estimate reflection spectra using 928 colors in the ISO12642 IT8/3 chart using a clustering and polynomial regression method.

An image of the X-rite ColorChecker standard (Macbeth) has been recorded in this manner using the VideometerLab system. Since only 11 of the bands created by the camera resides in the visible spectrum, these are the only ones containing color information, which is why the rest are discarded, weighted down, and not used further in this study. Finally the acquired multispectral image is seen in Figure 2 with 11 distinct wavelengths at; 430, 450, 470, 505, 525, 565, 590, 630, 645, 660, and 700 nanometer.

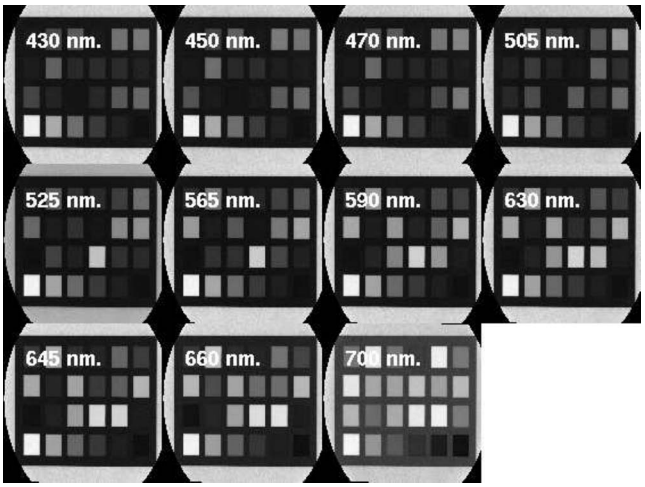

Figure 2. 11 Channels of a multispectral image containing a total of 20 channels. The wavelength at which the channel was recorded is shown on each image. The image was recorded using the VideometerLab with an LED technology.

As seen, the x-rite standard contains a matrix of colors, four rows and six columns, which sums to a total of 24 squares. These squares are extracted from the image manually, and a median value is calculated for each square thus yielding a total of 24 spectral samples. The real values of the colors in sRGB and CIE-Laboratory space are known, and can thus be used for calibration, which will be discussed further in the theory section.

THEORY

The relationship between spectral space and the three dimensional CIE-XYZ space is known to be linear [Eq. (1)]. Therefore we are able to map the spectra of the multispectral image seen in Fig. 2 into the CIE-XYZ using a linear model. For the duration of this section, the size of the spectral space will be denoted p, and the amount of samples is denoted N. A standard linear model is written on the form 2;

$$y(x) = \beta_0 + \beta_1 x_1 + \beta_2 x_2 + \cdots + \beta_p x_p + \epsilon. \tag{2}$$

Here y denotes the response, which we want to be able to predict, in this case a known CIE-XYZ value. x denotes the independent covariates, here a sparsely recorded electromagnetic spectrum. Since we do not know the exact relation between x and y, it is desirable to compute a set of adjustable parameters β in such a way that ϵ becomes as small as possible using a set of measured/observed spectra and a known target. If there exists more spectra samples than recorded wavelengths for each sample, the system is overdetermined, and several solutions exists, which is why the best approximate solution have to be determined.

Equation (2) resembles a plane in a hyperdimensional space, which we want to fit by minimizing the Euclidian distances between a given set of observations and the plane. This fit is often written as the residual sum of squares and is normally known as the ordinary least square (OLS) method [Eq. (3)];

$$\hat{\beta} = \arg\min_{\beta} \left\{ \sum_{i=1}^{N} \left(y_i - \beta_0 - \sum_{j=1}^{p} x_{ij}\beta_j \right)^2 \right\}. \tag{3}$$

The fastest way to minimize Eq. (3) is by setting the derive to 0 and solve for beta since this is a strictly convex problem. Written in matrix form, normally referred to as *the normal equations*, this may be written as

$$\hat{\beta} = (\mathbf{X}^T\mathbf{X})^{-1}\mathbf{X}^T\mathbf{y}, \tag{4}$$

where $\hat{\beta}$ is a $px3$ projection vector which is capable of projecting new x observations in p dimensional space into the three dimensional color space; $\hat{y}=\mathbf{X}\beta$, where $\mathbf{X}$ is the multispectral data and $\mathbf{y}$ is the matrix containing the true color values.

According to the Gauss-Markov theorem, the estimate of β in an OLS is the best linear unbiased estimator (BLUE), which means that for all unbiased solutions, the OLS solution is the one with smallest variance. However, the OLS problem may be modified to get biased estimators and thereby get an even better solution. A well known method used to modify the OLS in order to be able to solve ill-posed problems of overdetermined systems where the Gramian matrix $(\mathbf{X}^T\mathbf{X})$ is singular is the Tikhonov regularization[23,31,32] method—also known as ridge regression. This regularization basically penalizes the L2-norm or Euclidian length of the parameter vector, as seen below

$$\hat{\beta}^{\text{ridge}} = \arg\min_{\beta} \left\{ \sum_{i=1}^{N} \left(y_i - \beta_0 - \sum_{j=1}^{p} x_{ij}\beta_j \right)^2 \right\},$$

$$st \sum_{j=1}^{p} \beta_j^2 \leq s, \tag{5}$$

where s is thus a parameter that basically controls the bias-variance tradeoff as best as possible, meaning that this regularization makes it possible to find a biased solution with smaller variance than the BLUE estimate. The parameter s is chosen so that the generalization error is minimized, which in other terms means the best fit which is not an overfit. How this is done is described in the end of this section.

Since the Tikhonov regularization is a constraint version of the convex OLS problem, this leads to a quadratic constrained optimization problem. Such a problem may be solved in different ways, e.g., using quadratic programming with constraints or by solving the Lagrangian problem, by introducing a Lagrange multiplier λ in Eq. (5). After λ has been introduced, the formulation may again be recast to matrix form;

$$\hat{\beta} = (\mathbf{X}^T\mathbf{X} + \lambda\mathbf{I})^{-1}\mathbf{X}^T\mathbf{y}, \tag{6}$$

where $\mathbf{I}$ is the $p \times p$ identity matrix. The penalty term of the ridge regression shrinks the coefficients toward zero and thereby weighs down badly influencing variables more than others.

Instead of shrinking the length of the coefficient vector, we are interested in penalizing large variance between neighboring coefficients in order to obtain a more smooth coefficient/weight curve. We present a term based on the common finite difference operators, which are used to approximate numerical derivatives of arbitrary order. A penalization of the gradient of the coefficients β, is thus equivalent to a penalization of the backward finite difference of the coefficients

$$\nabla_h[f](x) = f(x) - f(x-h), \tag{7}$$

where h is set to step a single unit. Rewritten into a constraint, this is given as

$$\sum_{j=1}^{p-1} (\beta_j - \beta_{j+1})^2 \leq s. \tag{8}$$

Similarly a smoothing term could be incorporated as

$$\sum_{j=1}^{p-2} (\beta_j - 2\beta_{j+1} + \beta_{j+2})^2 \leq s. \tag{9}$$

Both terms should have the effect of preventing large fluctuations in the coefficients and make it easier to understand how the model predicts. In Ref. 24, the authors proposed a similar penalization, however with the L1-norm instead, which gives rise to piecewise linear sparse models which not is interesting in the type of problem we are dealing with in this article. Before this regularization may be used we have to assume an ordering of the coefficients β, which comes naturally for spectral data, since the coefficients represents neighboring wavelengths. Building the regularization into the OLS of a curvature penalization yields

$$\hat{\beta} = \arg\min_{\beta} \left\{ \sum_{i=1}^{N} \left(y_i - \beta_0 - \sum_{j=1}^{p} x_{ij}\beta_j \right)^2 \right\},$$

$$st \sum_{j=1}^{p-2} (\beta_j - 2\beta_{j+1} + \beta_{j+2})^2 \leq s. \tag{10}$$

Again we can rewrite this into Lagrangian form

$$\hat{\beta} = (\mathbf{X}^T\mathbf{X} + \lambda\mathbf{A}^T\mathbf{A})^{-1}\mathbf{X}^T\mathbf{y}, \tag{11}$$

where $\mathbf{A}$ is a $p \times p$ tridiagonal matrix;

$$\mathbf{A} = \begin{bmatrix} 1 & -2 & 1 & 0 & \dots & 0 \\ 0 & 1 & -2 & 1 & \dots & 0 \\ \vdots & \vdots & \vdots & \ddots & \vdots & \vdots \\ 0 & 0 & \dots & 1 & -2 & 1 \\ 0 & 0 & \dots & 0 & 0 & 0 \\ 0 & 0 & \dots & 0 & 0 & 0 \end{bmatrix}. \tag{12}$$

Due to the sparse amount of observations, leave one out cross validation (LOOCV) is used to evaluate the model and calculate the generalization error.[33] This means the model is trained and evaluated n times, one time for each sample, with all observations except the left out sample which is used to generate a test-error residual. Finally a total test error can be calculated. A finite difference or gradient descend scheme was used to select proper parameter values for the regularization parameters.

EXPERIMENTAL DATA AND RESULTS

Having a multispectral image of a color checker with 24 different color patches recorded at 11 different wavelengths means we have $n=24$ observations and $p=11$ variables and thus an overdetermined system. 24 patches are very few observations in a regression method, and care should be taken not to overfit the data, which we have chosen to avoid by minimizing the test error with LOOCV and a finite difference scheme, as described in the previous section. Before the calibration, all real color patch values were transformed from CIE-Laboratory to CIE-XYZ using

$$Y = \begin{cases} Y_n f_y^3 & \text{for } f_y > \delta \\ f_y - \frac{16}{116} 3\delta^2 Y_n & \text{otherwise,} \end{cases} \qquad f_y \equiv \frac{L^* + 16}{116},$$

$$X = \begin{cases} X_n f_x^3 & \text{for } f_x > \delta \\ f_x - \frac{16}{116} 3\delta^2 X_n & \text{otherwise,} \end{cases} \qquad f_x \equiv f_y + \frac{a^*}{500},$$

$$Z = \begin{cases} Z_n f_z^3 & \text{for } f_z > \delta \\ f_z - \frac{16}{116} 3\delta^2 Z_n & \text{otherwise,} \end{cases} \qquad f_z \equiv f_y - \frac{b^*}{200},$$

$$\delta = \frac{6}{29}, \tag{13}$$

with the D50, 2° observer white spot reference.

Four different regression schemes were compared, i.e., least-squares, ridge regression, gradient ridge regression (GRR), and curvature ridge regression (CRR), all presented in the theory section. In order to compare the results, we report the min, max, and mean ΔE of the color reconstructions;

$$\Delta E = \sqrt{(L_1 - L_2)^2 + (a_1 - a_2)^2 + (b_1 - b_2)^2}, \tag{14}$$

as well as mean Euclidian distance in XYZ space, denoted $\overline{\Delta XYZ}$ and finally the test root mean square error.

For the penalized regression schemes, a λ was chosen for each channel, resulting in a total of three λ per regression scheme. Table I shows a compilation of the results, the best being underlined.

From Table I it is seen that the OLS method attains the lowest $\overline{\Delta E}$ error of 1.29. This is however not the case with the $\overline{\text{RMS}}$. This is worth noticing and is caused by the fact that all the applied procedures minimizes RMS and not $\overline{\Delta E}$,

Table I. Resulting colorimetric errors using four different regression methods on 11 different wavelengths. All errors are generalization errors calculated using leave one out cross validation.

	ΔE_{MIN}	ΔE_{MAX}	$\overline{\Delta E}$	$\overline{RMS}$	$\overline{\Delta XYZ}$
OLS	0.24431	3.9309	1.2912	0.75088	0.58368
RR	0.26119	4.6468	1.3993	0.66173	0.64521
GRR	0.25967	4.5934	1.3191	0.64494	0.60110
CRR	0.26384	4.6233	1.3249	0.64973	0.60863

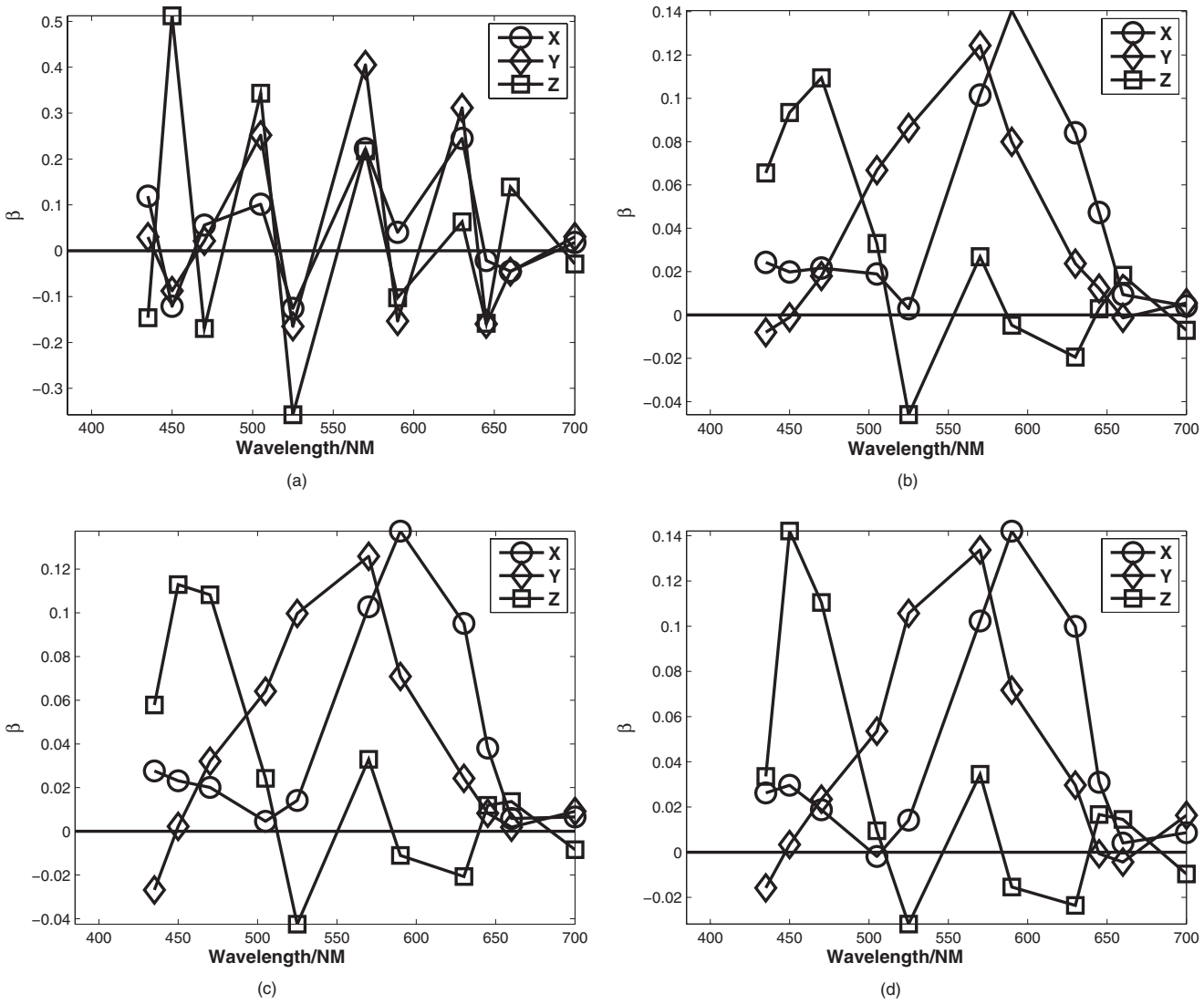

Figure 3. (a) Ordinary least-squares fit, (b) ridge regression fit, curvature penalization fit of first derivative, and (c) curvature penalization fit of second derivative.

which has a nonlinear relationship. Aside from OLS, the other procedures attains more or less equal error magnitude in CIE-Laboratory space. It is furthermore worth noticing that all methods attain mean LAB differences below 3, which according to Ref. 3 as a rule of thumb is *Hardly perceptible* by the human eye. Figure 3 shows plots of the calculated coefficients for each of the four tested regression methods. OLS clearly stand out, with coefficient the does not show any particular pattern. The three regularized regression schemes however shows a clear correlation with the CIE-XYZ tristimuli curves, which would make sense to obtain in a regression of a problem as the one posed in this article. The blue tristimuli model seems however a bit oscillating, while the red and green models seems to be shifted a bit in the spectrum compared to the real tristimuli functions. The coefficients of the three regularized methods seem quite similar, especially the penalization of the gradient and curvature methods, which naturally both seem to be a bit more smooth than ridge regression. In case we had densely sampled hyperspectral images we would be able to directly

use the theoretical *XYZ* tristimulus values to map the spectra into the *XYZ* color space. However, having sparsely sampled spectra this is not an option and as an alternative to reconstructing spectra using any existing method, the smooth regularization shown in Fig. 3 shows that we are able to create sensible substitution weighting curves to the theoretical *XYZ* tristimulus curves. Thus, these curves are able to map sparsely sampled multispectral images into *XYZ* space in the same way the theoretical curves maps densely sampled spectra using Eq. (1).

CONCLUSION

The focus of this article has been to develop an alternative method to map a multispectral image into the independent colorimetric color space, CIE XYZ. The method is built to support a multispectral image of arbitrary spectral dimensionality, above three and specifically tested on a multispectral system with 11 wave bands in the visible area. To create a projection vector, a regularized regression technique was utilized and evaluated on the x-rite ColorChecker Chart containing 24 different color patches using leave one out cross validation. The cross validation enabled us to assess the generalization ability in spite of the few color samples available. The colorimetric prediction ability was reported in $\overline{\Delta E}$, RMS, and ΔXYZ and yielded good and interpretable color reproduction results. A drawback of this method is that in order to calculate proper weights of the projection vector, β, it is necessary to do the regression on reflection spectra from a training image with the same light setup as the target image. By light setup for the used multispectral system, is meant the amount of power going through the light emitting diodes, as well as the strobing time which is optimized for best dynamic range in a local area of a given surface chemistry. However, for any other multispectral system, the training and target image would have to be recorded under the same lighting conditions, which usually is possible.

For correct light setups, the reported results, all with $\overline{\Delta E}$ values below 3, indicate a hardly perceptible error between the real color checker values and the estimation provided by the mapping method. Plots of the estimated regularized models motivated a regularization approach to achieve higher interpretability, while colorimetric measures showed that ordinary least square better predictions performed slightly better.

REFERENCES

[1] G. Wyszecki and W. S. Stiles, *Color Science: Concepts and Methods, Quantitative Data, and Formulas*, 2nd ed. (Wiley & Sons, New York, 2000).
[2] H. Grassmann, "Zur theorie der farbenmischung", Ann. Phys. **165**, 69–84 (1853).
[3] J. Y. Hardeberg, "Acquisition and reproduction of color images: Colorimetric and multispectral approaches", Ph.D. thesis, Ecole Nationale Superieure des Telecommunications, 2001.
[4] J. Brauers, N. Schulte, and T. Aach, "Multispectral filter-wheel cameras: Geometric distortion model and compensation algorithms", IEEE Trans. Image Process. **17**, 2368–2380 (2008).
[5] J. Y. Hardeberg, F. J. Schmitt, and H. Brettel, "Multispectral color image capture using a liquid crystal tunable filter", Opt. Eng. **41**, 2532–2548 (2002).
[6] N. Gat, "Imaging spectroscopy using tunable filters: A review", Proc. SPIE **4056**, 50–64 (2000).
[7] URL, http://www.videometer.com.
[8] C. Connolly and T. Fliess, "A study of efficiency and accuracy in the transformation from rgb to cielab color space", IEEE Trans. Image Process. **6**, 1046–1048 (1997).
[9] P. C. Hung, "Colorimetric calibration for scanners and media", Proc. SPIE **1448**, 164–174 (1991).
[10] M. G. Hong, Ronnier Luo, and Peter A. Rhodes, "A study of digital camera colorimetric characterization based on polynomial modeling", Color Res. Appl. **26**, 76–84 (2001).
[11] T. L. V. Cheung, S. Westland, D. R. Connah, and C. Ripamonti, "A comparative study of the characterization of colour cameras by means of neural networks and polynomial transforms", J. Coloration Technol. **120**, 19–25 (2004).
[12] F. A. Kruse, A. B. Lefkoff, J. W. Boardman, K. B. Heidebrecht, A. T. Shapiro, P. J. Barloon, and A. F. H. Goetz, "The spectral image processing system (sips): Interactive visualization and analysis of imaging spectrometer data", Remote Sens. Environ. **44**, 145–163 (1993).
[13] N. P. Jacobson and M. R. Gupta, "Design goals and solutions for display of hyperspectral images", IEEE Trans. Geosci. Remote Sens. **43**, 2684–2692 (2005).
[14] A. Mansouri, T. Sliwa, J. Y. Hardeberg, and Y. Voisin, "Representation and estimation of spectral reflectances using projection on pca and wavelet bases", Color Res. Appl. **33**, 485–493 (2008).
[15] J. M. DiCarlo and B. A. Wandell, "Spectral estimation theory: Beyond linear but before Bayesian", J. Opt. Soc. Am. **20**, 1261–1270 (2003).
[16] N. Tsumura, H. Sato, T. Hasegawa, H. Haneishi, and Y. Miyake, "Limitation of color samples for spectral estimation from sensor responses in fine art painting", Opt. Rev. **6**, 57–61 (1999).
[17] Y. Zhao, M. Nezamabadi, L. A. Taplin, and R. S. Berns, "Using the matrix *r* method for spectral image archives", Tenth Congress of the International Color Association, 2005 (unpublished).
[18] D. R. Connah and J. Y. Hardeberg, "Spectral recovery using polynomial models", Proc. SPIE **5667**, 65–75 (2004).
[19] P. Stigell, K. Miyata, and M. Hauta-Kasari, "Wiener estimation method in estimating of spectral reflectance from rgb images", Pattern Recognition and Image Analysis **17**, 233–242 (2007).
[20] D. Nystrom, "Colorimetric and multispectral image acquisition using model-based and empirical device characterization", in *SCIA*, Lecture Notes in Computer Science, Vol. **4522**, edited by Bjarne K. Ersboll and Kim Steenstrup Pedersen (Springer, New York, 2007) pp. 798–807.
[21] J. Conde, H. Haneishi, M. Yamaguchi, N. Ohyama, and J. Baez, "Cie-xyz fitting by multispectral images and mean square error minimization with a linear interpolation function", Rev. Mex. Fis. **50**, 601–607 (2004).
[22] J. Y. Hardeberg, F. J. Schmitt, and H. Brettel, "Multispectral image capture using a tunable filter", Proc. SPIE **3963**, 78–88 (1999)
[23] A. E. Hoerl and R. W. Kennard, "Ridge regression: Biased estimation for nonorthogonal problems", Technometrics **12**, 55–67 (1970).
[24] R. Tibshirani, M. Saunders, S. Rosset, J. Zhu, and K. Knight, "Sparsity and smoothness via the fused lasso", J. R. Stat. Soc. Ser. B (Stat. Methodol.) **67**, 91–108 (2005).
[25] URL, http://www.xrite.com.
[26] C. S. McCamy, H. Marcus, and J. G. Davidson, "A color-rendition chart", J. Appl. Photogr. Eng. **2**, 95–99 (1976).
[27] B. S. Dissing, L. H. Clemmesen, H. Løje, B. K. Ersbøll, and J. Adler-Nissen, "Temporal reflectance changes in vegetables", Proceedings of IEEE Color and Reflectance in Imaging and Computer Vision Workshop, Kyoto, Japan, 2009 (unpublished).
[28] L. H. Clemmesen and B. K. Ersbøll, "Multispectral recordings and analysis of psoriasis lesions", MICCAI '06-Workshop on Biophotonics Imaging for Diagnostics and Treatment: 9th MICCAI Conference, 2006 (unpublished) pp. 15–18.
[29] M. E. Hansen, B. K. Ersbøll, J. M. Carstensen, and A. A. Nielsen, Lect. Notes Comput. Sci. **3540**, 1228–1237 (2005).
[30] S. Yamamoto, N. Tsumura, T. Nakaguchi, and Y. Miyake, "Development of a multispectral scanner using led array for digital color proof", J. Imaging Sci. Technol. **51**, 61–69 (2007).
[31] A. N. Tikhonov, "Solutions of incorrectly formulated problems and the regularization method", Sov. Math. Dokl. **4**, 1035–1038 (1963) [Akad. Nauk. SSSR **151**, 501–504 (1963)].
[32] T. Hastie, R. Tibshirani, and J. Friedman, *Elements of Statistical Learning: Data mining, inference, and prediction* (Springer-Verlag, New York, 2001).
[33] H. A. Martens and P. Dardenne, "Validation and verification of regression in small data sets", Chemom. Intell. Lab. Syst. **44**, 99–121 (1998).